GEOCHEMISTRY

Crustal thickening and endogenic oxidation of magmatic sulfur

Ming Tang[1,2]*, Cin-Ty A. Lee[2]*, Wei-Qiang Ji[3], Rui Wang[4], Gelu Costin[2]

Porphyry ore deposits, Earth's most important resources of copper, molybdenum, and rhenium, are strongly associated with felsic magmas showing signs of high-pressure differentiation and are usually found in places with thickened crust (>45 kilometers). This pattern is well-known, but unexplained, and remains an outstanding problem in our understanding of porphyry ore deposit formation. We approach this problem by investigating the oxidation state of magmatic sulfur, which controls the behavior of ore-forming metals during magma differentiation and magmatic-hydrothermal transition. We use sulfur in apatite to reconstruct the sulfur oxidation state in the Gangdese batholith, southern Tibet. We find that magma sulfate content increased abruptly after India-Eurasia collision. Apatite sulfur content and the calculated magma $S^{6+}/\Sigma S$ ratio correlate with whole-rock dysprosium/ytterbium ratio, suggesting that residual garnet, favored in thickened crust, exerts a first-order control on sulfur oxidation in magmatic orogens. Our findings link sulfur oxidation to internal petrogenic processes and imply an intrinsic relationship of magma oxidation with synmagmatic crustal thickening.

INTRODUCTION

The oxidation state of sulfur (S) strongly influences its cycling in subduction zones and the transport and enrichment of ore-forming chalcophile elements in the crust. Porphyry ore deposits are closely related to sulfate-rich magmatic plutons in convergent margins (*1*, *2*), but where the oxidized S is sourced from remains elusive. One possibility is that the sulfate comes from subducted slab, which, in turn, is derived from oxidized sediments or seawater (*3*, *4*). However, sedimentary and seawater sulfate has distinctively heavy sulfur isotopes (*5*), which are not seen in most porphyry ore deposits. The bulk sulfur of porphyry systems generally has near-mantle isotopic ratios (*6*, *7*), suggesting that the sulfur budget derives from mantle sulfides instead of subducted sulfate. The recent work by Li *et al.* (*8*) further demonstrates that the sulfate released from subducted slab is negligible.

Clues to the mysterious sulfate may come from the observation that porphyry ore deposits are preferentially found in places with thickened crust. For example, porphyry copper deposits are commonly seen in continental arcs and continental collision zones but rare in immature island arcs (*1*). This empirical relationship hints at a link between crustal thickening and high magmatic sulfate contents/S oxidation state. Below, we use a case study of southern Tibet to evaluate this hypothesis and explore the underlying petrologic mechanism.

Geologic background and samples

Southern Tibet has the thickest continental crust (60 to 80 km) in the world. This phenomenal crustal thickness was achieved about 30 million years (Ma) ago after the Indian continent collided with the Eurasian continent (*9*). Before the collision, southern Tibet had been a convergent margin associated with northward subduction of the Neo-Tethyan oceanic lithosphere since the Mesozoic (*10*). Magmatic activity in southern Tibet dates back to the Triassic and continued through the Miocene (*11*, *12*). The >200-Ma interval of magmatism, consisting of subduction and postcollision phases, produced the massive Gangdese batholith, spanning more than 1500 km along the India-Eurasia suture zone (Fig. 1A).

The Gangdese batholith hosts multiple giant porphyry Cu-Mo deposits, but almost all of the Gangdese porphyry deposits are associated with young magmatism within the past 30 Ma (*13*, *14*) (Fig. 1B). It is intriguing that the Gangdese porphyry ore deposits primarily formed after the India-Eurasia collision but were scarce in the subduction stage (*14*, *15*). However, from another perspective, mineralization in the Gangdese was contemporaneous with intense crustal thickening, a pattern that corroborates the global observations (*1*, *16*–*19*).

We sampled 22 plutons covering the entire 1500-km-long Gangdese belt (Fig. 1A). Our samples are I-type unmineralized granitic rocks with whole-rock SiO_2 content between 61 and 71 weight % (see the Supplementary Materials). They are likely produced by partial remelting of the juvenile Gangdese lower crust (*20*). The ages of our samples range from 90 to 16 Ma and thus cover the magmatisms from subduction to postcollision phases in the Gangdese belt.

Sulfur in apatite as an indicator of magmatic sulfate content

Because S partitioning into apatite is highly dependent on the oxidation state of S in the silicate melt but mostly independent of temperature and pressure (*21*, *22*), apatite S content may be used as a proxy for S oxidation state in the melt. Under reduced conditions, S in the melt is dominated by S^{2-}, which is incompatible in apatite, so S does not exceed a few hundred parts per million (ppm) in apatite; under oxidized conditions, S is present predominantly as sulfate (SO_4^{2-}) in the melt, which is compatible in apatite and leads to high apatite S contents (>1000 ppm) (*21*, *23*). Sulfur of intermediate oxidation states (S^{1+} and S^{4+}) may also exist in the melt, but they are far less abundant compared with S^{6+}, and their incorporation in apatite is trivial (*23*, *24*). In the apatite lattice, SO_4^{2-} may substitute for PO_4^{3-} by charge coupling with SiO_4^{4-} (*25*), which may complicate the use of S content in apatite as an indicator of sulfate content in melts with a wide range of compositions. We suggest that in felsic magmatic systems where the melt is quartz-saturated or close to quartz saturation, SiO_2 activity is relatively fixed, and charge coupling with SiO_4^{4-} would have a constant effect on S content in apatite. In this case, the variation of S content in apatite is chiefly governed by sulfate content in the melt.

[1]School of Earth and Space Sciences, Peking University, Beijing 100871, China. [2]Department of Earth, Environmental and Planetary Sciences, Rice University, Houston, TX 77005, USA. [3]State Key Laboratory of Lithospheric Evolution, Institute of Geology and Geophysics, Chinese Academy of Sciences, P.O. Box 9825, Beijing 100029, China. [4]State Key Laboratory of Geological Processes and Mineral Resources, and Institute of Earth Sciences, China University of Geosciences, Beijing 100083, China.
*Corresponding author. Email: mingtang@pku.edu.cn (M.T.); ctlee@rice.edu (C.-T.A.L.)

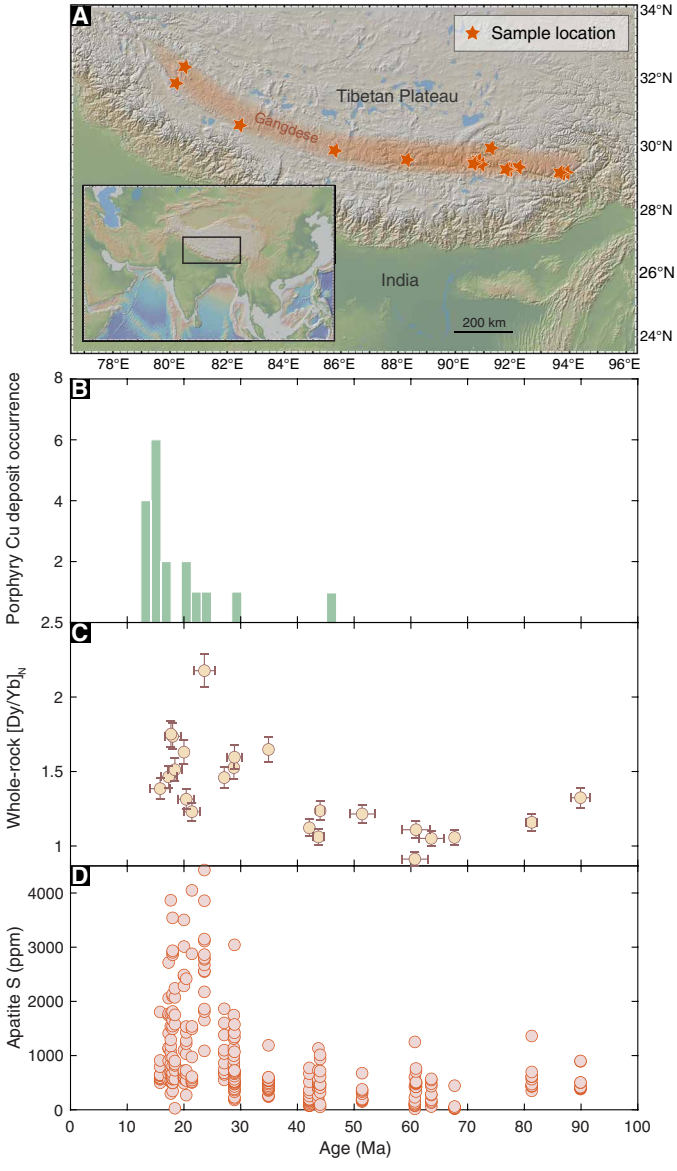

Fig. 1. Map, mineralization history, and geochemical evolution of the Gangdese batholith, southern Tibet. (**A**) Map of southern Tibet and sample locations. The map was made using GeoMapApp (http://geomapapp.org). (**B**) Occurrence of Cu porphyry deposits from (*13*, *15*, *53*–*57*). (**C**) Whole-rock $[Dy/Yb]_N$. The subscript N denotes C1 chondrite normalized (*58*). The uncertainties of U-Pb ages in (C) are 95% confidence-weighted errors. For some samples, the error bars are smaller than the symbols; the uncertainties of whole-rock $[Dy/Yb]_N$ in (C) are 5%. (**D**) Apatite S contents. The error bars of S measurements are similar to or smaller than the symbols.

RESULTS AND DISCUSSION

The Gangdese plutons document correlated evolution of magma Dy/Yb ratio, apatite S content, and the mineralization history (Fig. 1). The fractionation between rare earth elements (REEs) is sensitive to magmatic differentiation pressure, which, in turn, increases systematically with increasing thickness of the overlying crust (*26*–*28*). At low pressure, the residual/fractionating assemblage is dominated by plagioclase, amphibole, and pyroxene, all of which have near-flat REE partition coefficient patterns (*29*). At high pressure, garnet is stable and strongly fractionates heavy REEs from middle REEs because of garnet's strong preference for heavy REEs (*30*), resulting in an increase in middle-to-heavy REE ratios, such as Dy/Yb. Rapid crustal thickening in the Neogene is reflected by a rapid increase in the Dy/Yb of postcollision plutons younger than 30 Ma (Fig. 1C). An earlier crustal thickening event at 80 to 70 Ma in the Lhasa terrane has also been suggested by some researchers (*31*), but it is not seen here due to lack of samples within that time window.

Apatite S contents are highly variable within each sample, particularly in the postcollision plutons. We do not know what causes the within-sample S variability. One possibility is that S (both S^{2-} and SO_4^{2-}) was being extracted from the melt by exsolving fluids (*32*, *33*) during apatite crystallization. Alternatively, the highly variable S content in apatite may be due to small fluctuations in oxygen fugacity near the narrow sulfate-sulfide transition, which can markedly change the bulk S partitioning coefficient between apatite and melt. Both of these processes lead to lower apatite S contents. Nevertheless, we see that Neogene crustal thickening is attended by a systematic increase in apatite S contents from the Gangdese batholith (Fig. 1D). In the precollision plutons (>50 Ma), apatite S contents are generally lower than 1000 ppm, whereas in the postcollision plutons (<30 Ma), apatite S contents reach up to 4500 ppm.

Because S only becomes compatible in apatite when it is oxidized to sulfate (*24*), we interpret the high apatite S contents of the postcollision plutons in the Gangdese batholith as reflecting high magmatic sulfate contents. The rise in apatite S content at ~30 Ma suggests that magma S oxidation became pervasive only after extensive crustal thickening. The correlation between S oxidation and crustal thickness is reinforced by the observation that apatite S contents show no correlation with differentiation or source compositions but instead correlate with whole-rock Dy/Yb ratio (Fig. 2). The lack of correlation between apatite S content and whole-rock SiO_2 content (Fig. 2A) reaffirms that charge coupling with SiO_4^{2-} has little influence on S content in apatite in felsic systems.

The correlation between apatite S content and whole-rock Dy/Yb ratio links S oxidation to garnet, a residual/fractionating phase that only occurs at high pressure. The connection to garnet is of interest because garnet fractionation strongly depletes ferrous Fe but not ferric Fe from the melt, causing melt $Fe^{3+}/\Sigma Fe$ ratio to rise (*34*). Because Fe is a major source of electron transfer in magmatic systems, elevated $Fe^{3+}/\Sigma Fe$ in the melt should increase oxygen fugacity, which may in turn lead to the oxidation of other multivalence elements at lower abundance, such as S.

We now explore how S oxidation state and Dy/Yb ratio in the melt in equilibrium with residual garnet evolves during lower crust melting. We first estimate melt $S^{6+}/\Sigma S$ using S contents in apatite and the empirical sulfate partitioning relationship between apatite and silicate melt (*22*). Because we do not know the precise S^{2-} contents in the melt, we use sulfur concentration at sulfide saturation under reduced conditions as the maximum S^{2-} content in the felsic melt (~200 ppm; see fig. S3 in the Supplementary Materials). Thereby, our estimated $S^{6+}/\Sigma S$ are minimum bounds.

To calculate the redox effect of residual garnet during crustal remelting, we assume that the lower crust is basaltic with 8.5 wt % FeO_T and $Fe^{3+}/\Sigma Fe$ of 0.16 before melting. These values are typical of slightly oxidized arc basalts (*35*). The melting residue is arclogitic, with clinopyroxene and garnet as the major Fe-bearing minerals. Clinopyroxene is in equilibrium with garnet such that $(Fe^{3+}/\Sigma Fe)_{clinopyroxene} = 2^*(Fe^{3+}/\Sigma Fe)_{garnet}$ (*36*). Sulfur oxidation state ($S^{6+}/\Sigma S$) can be calculated via S^{6+}/S^{2-}–Fe^{3+}/Fe^{2+} equilibrium (*37*) and electron conservation in

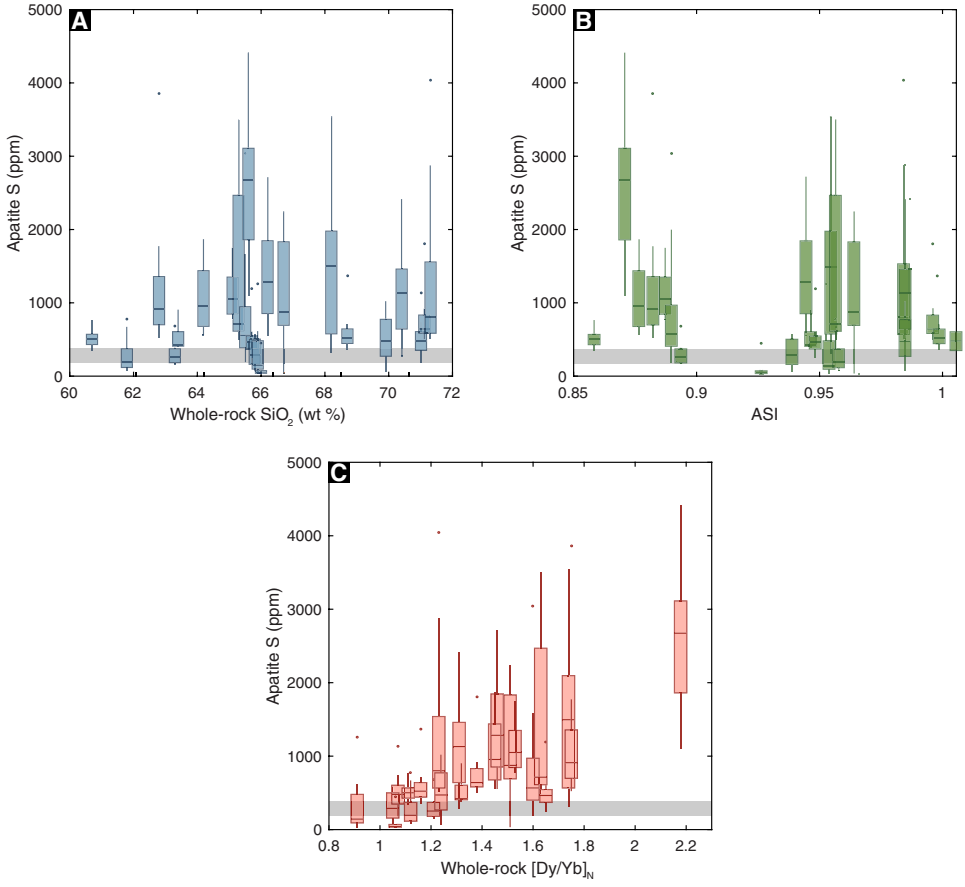

Fig. 2. Differentiation, source composition and residual garnet effects on apatite sulfur content. The data are presented as box and whisker plots of apatite S content versus pluton whole-rock SiO_2 content (**A**), aluminum saturation index (ASI) (**B**), and $[Dy/Yb]_N$ (**C**). The ends of the boxes show the upper and lower quartiles, and the ends of the whiskers show the 2.5 and 97.5 percentiles. Outliers are plotted as individual points. We also measured apatite in a mafic diorite sample (SiO_2 = 53 wt %) from the Gangdese batholith, whose S contents (160 to 320 ppm) are marked by the gray bar. This shows a baseline for apatite S contents in less differentiated samples.

the melt. Residual garnet leads to high $S^{6+}/\Sigma S$ and high Dy/Yb in the melt. For a reasonable range of garnet $Fe^{3+}/\Sigma Fe$ ratio (0.01 to 0.07) (*34*, *38*), our model can produce the melt $S^{6+}/\Sigma S$ ratios inferred from sulfate partitioning between apatite and silicate melt (*22*) and their correlations with magma Dy/Yb ratios (Fig. 3; see the Supplementary Materials). We acknowledge that some of the assumptions used above are loosely constrained, but as a proof of concept, our modeling exercise demonstrates that garnet fractionation alone can generate enough oxidizing power to convert sulfide to sulfate in the melt.

Implications

The increase in S oxidation state with crustal thickening has important implications for the geochemical behavior of chalcophile elements, such as Cu, which strongly partition into sulfides (*18*). Any sulfide segregation rapidly depletes Cu and other chalcophile metals from the melt. By contrast, high $S^{6+}/\Sigma S$ in the melt favors sulfate over sulfide, preventing extensive sulfide segregation and hence chalcophile element depletion during crystallization of the plutonic reservoir that feeds mineralization systems in the shallow crust. Hence, chalcophile metals remain in the melt, becoming more concentrated with progressive crystallization until the point of fluid saturation, after which pulsed fluid exsolution scavenges metals from the residual melts and concentrates them in mineralization traps (*39*, *40*).

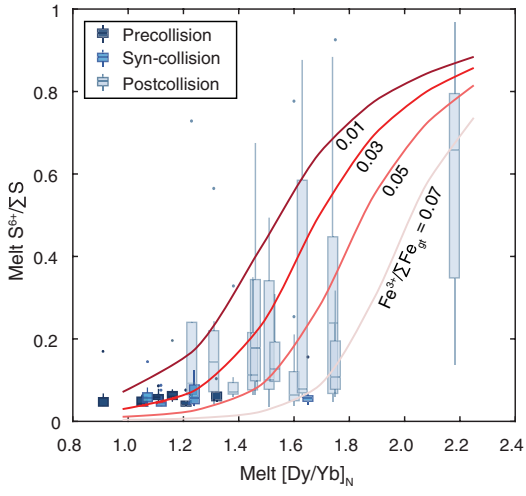

Fig. 3. Residual garnet effect on sulfur oxidation. We calculate the S^{6+} content in the melt using apatite S content and the empirical sulfate partitioning equation from (*22*). Calculated $S^{6+}/\Sigma S$ ratios are shown by box and whisker plots similar to Fig. 2. Superimposed are model curves for residual garnet effect on $S^{6+}/\Sigma S$ in the melt after 30% melting (see the Supplementary Materials). We consider a range of $Fe^{3+}/\Sigma Fe$ (0.01 to 0.07) (*34*, *38*) in the residual garnet, which determines the amount of Fe^{3+} in the melt available for S oxidation.

Endogenic sulfur oxidation points to the key role of orogenesis in the formation of porphyry ore deposits whether they are associated with collisional orogens such as Tibet or subduction orogens such as the Andean arc and North American Cordillera. This generality of endogenic oxidation during synmagmatic crustal thickening is supported by the prominent relationship between porphyry ore deposits and magmas with high-pressure differentiation signatures (e.g., high Sr/Y and La/Yb) around the world (*16*–*19*). Porphyry ore deposits may be a natural outcome in the evolution of magmatic orogens, and their formation may not require oxidized sources in the slab and mantle or the addition of oxidized supracrustal materials as often suggested (*4*, *41*).

Our findings highlight the importance of petrologic processes in the formation of porphyry ore deposits (*16*). Metal-enriched sources/magmas may contribute to the potential of ore deposit formation but are not a decisive factor. Most porphyry Cu deposits are found in continental arcs and collision zones where magmas are generally depleted in Cu (*16*, *18*, *42*).

A final implication of our findings relates to the S cycling on Earth's surface before the rise of atmospheric oxygen. In the Archean, sulfate supply was limited, and the seawater sulfate concentration was four orders of magnitude lower than today (*43*) due to the lack of atmospheric oxygen and thus large-scale oxidative weathering on land (*44*–*47*). There may have been times in the Archean that were characterized by widespread orogenesis, such as during craton formation (*48*–*50*). Sulfur oxidation in these magmatic orogens may have provided an important mechanism for generating and transporting sulfate to the Archean surface environment in the absence of oxidative weathering. Sulfate fuels a number of metabolic processes and drives oxidation in the marine environment when buried as sulfide (*51*, *52*). We thus suggest that the rise and fall of magmatic orogens may have played an important role in modulating the redox state of the Archean marine environment.

MATERIALS AND METHODS

Details about the samples, analytical techniques, and modeling are provided in the Supplementary Materials. Data are provided in data file S1.

SUPPLEMENTARY MATERIALS

Supplementary material for this article is available at http://advances.sciencemag.org/cgi/content/full/6/31/eaba6342/DC1

REFERENCES AND NOTES

1. R. H. Sillitoe, Porphyry copper systems. *Econ. Geol.* **105**, 3–41 (2010).
2. J. P. Richards, The oxidation state, and sulfur and Cu contents of arc magmas: Implications for metallogeny. *Lithos* **233**, 27–45 (2015).
3. K. A. Evans, The redox budget of subduction zones. *Earth Sci. Rev.* **113**, 11–32 (2012).
4. D. A. Stolper, C. E. Bucholz, Neoproterozoic to early Phanerozoic rise in island arc redox state due to deep ocean oxygenation and increased marine sulfate levels. *Proc. Natl. Acad. Sci. U.S.A.* **116**, 8746–8755 (2019).
5. A. Paytan, M. Kastner, D. Campbell, M. H. Thiemens, Seawater sulfur isotope fluctuations in the Cretaceous. *Science* **304**, 1663–1665 (2004).
6. W. C. Pat Shanks, in *Treatise on Geochemistry (Second Edition)*, H. D. Holland, K. K. Turekian, Eds. (Elsevier, 2014), pp. 59–85.
7. H. Ohmoto, Stable isotope geochemistry of ore deposits, in *Stable Isotopes in High Temperature Geological Processes. Reviews in Mineralogy*, J. W. Valley, H. P. Taylor Jr., J. R. O'Neil, Eds. (Washington, DC: Mineralogical Society of America, 1986), vol. 16, pp. 491–559.
8. J.-L. Li, E. M. Schwarzenbach, T. John, J. J. Ague, F. Huang, J. Gao, R. Klemd, M. J. Whitehouse, X.-S. Wang, Uncovering and quantifying the subduction zone sulfur cycle from the slab perspective. *Nat. Commun.* **11**, 514 (2020).
9. D.-C. Zhu, Q. Wang, P. A. Cawood, Z.-D. Zhao, X.-X. Mo, Raising the Gangdese Mountains in southern Tibet. *J. Geophys. Res. Solid Earth* **122**, 214–223 (2017).
10. C. J. Allégre, V. Courtillot, P. Tapponnier, A. Hirn, M. Mattauer, C. Coulon, J. J. Jaeger, J. Achache, U. Schärer, J. Marcoux, J. P. Burg, J. Girardeau, R. Armijo, C. Gariépy, C. Göpel, L. Tindong, X. Xuchang, C. Chenfa, L. Guangqin, L. Baoyu, T. Jiwen, W. Naiwen, C. Guoming, H. Tonglin, W. Xibin, D. Wanming, S. Huaibin, C. Yougong, Z. Ji, Q. Hongrong, B. Peisheng, W. Songchan, W. Bixiang, Z. Yaoxiu, R. Xu, Structure and evolution of the Himalaya–Tibet orogenic belt. *Nature* **307**, 17–22 (1984).
11. M.-F. Chu, S.-L. Chung, B. Song, D. Liu, S. Y. O'Reilly, N. J. Pearson, J. Ji, D.-J. Wen, Zircon U-Pb and Hf isotope constraints on the Mesozoic tectonics and crustal evolution of southern Tibet. *Geology* **34**, 745–748 (2006).
12. W.-Q. Ji, F.-Y. Wu, S.-L. Chung, J.-X. Li, C.-Z. Liu, Zircon U–Pb geochronology and Hf isotopic constraints on petrogenesis of the Gangdese batholith, southern Tibet. *Chem. Geol.* **262**, 229–245 (2009).
13. Z. Hou, Z. Yang, X. Qu, X. Meng, Z. Li, G. Beaudoin, Z. Rui, Y. Gao, K. Zaw, The Miocene Gangdese porphyry copper belt generated during post-collisional extension in the Tibetan Orogen. *Ore Geol. Rev.* **36**, 25–51 (2009).
14. R. Wang, R. F. Weinberg, W. J. Collins, J. P. Richards, D.-c. Zhu, Origin of postcollisional magmas and formation of porphyry Cu deposits in southern Tibet. *Earth Sci. Rev.* **181**, 122–143 (2018).
15. Z. Hou, L. Duan, Y. Lu, Y. Zheng, D. Zhu, Z. Yang, Z. Yang, B. Wang, Y. Pei, Z. Zhao, T. C. McCuaig, Lithospheric architecture of the Lhasa terrane and its control on ore deposits in the Himalayan-Tibetan orogen. *Econ. Geol.* **110**, 1541–1575 (2015).
16. C.-T. A. Lee, M. Tang, How to make porphyry copper deposits. *Earth Planet. Sci. Lett.* **529**, 115868 (2020).
17. M. Chiaradia, A. Ulianov, K. Kouzmanov, B. Beate, Why large porphyry Cu deposits like high Sr/Y magmas? *Sci. Rep.* **2**, 685 (2012).
18. C.-T. A. Lee, P. Luffi, E. J. Chin, R. Bouchet, R. Dasgupta, D. M. Morton, V. Le Roux, Q.-z. Yin, D. Jin, Copper Systematics in Arc Magmas and Implications for Crust-Mantle Differentiation. *Science* **336**, 64–68 (2012).
19. R. R. Loucks, Distinctive composition of copper-ore-forming arcmagmas. *Aust. J. Earth Sci.* **61**, 5–16 (2014).
20. Z.-Q. Hou, Y.-F. Gao, X.-M. Qu, Z.-Y. Rui, X.-X. Mo, Origin of adakitic intrusives generated during mid-Miocene east–west extension in southern Tibet. *Earth Planet. Sci. Lett.* **220**, 139–155 (2004).
21. G. Peng, J. F. Luhr, J. J. McGee, Factors controlling sulfur concentrations in volcanic apatite. *Am. Mineral.* **82**, 1210–1224 (1997).
22. F. Parat, F. Holtz, M. J. Streck, Sulfur-bearing magmatic accessory minerals. *Rev. Mineral. Geochem.* **73**, 285–314 (2011).
23. B. A. Konecke, A. Fiege, A. C. Simon, F. Parat, A. Stechern, Co-variability of S6+, S4+, and S2− in apatite as a function of oxidation state: Implications for a new oxybarometer. *Am. Mineral.* **102**, 548–557 (2017).
24. B. A. Konecke, A. Fiege, A. C. Simon, S. Linsler, F. Holtz, An experimental calibration of a sulfur-in-apatite oxybarometer for mafic systems. *Geochim. Cosmochim. Acta* **265**, 242–258 (2019).
25. R. C. Rouse, P. J. Dunn, A contribution to the crystal chemistry of ellestadite and the silicate sulfate apatites. *Am. Mineral.* **67**, 90–96 (1982).
26. L. Profeta, M. N. Ducea, J. B. Chapman, S. R. Paterson, S. M. H. Gonzales, M. Kirsch, L. Petrescu, P. G. DeCelles, Quantifying crustal thickness over time in magmatic arcs. *Sci. Rep.* **5**, 17786 (2015).
27. M. J. Farner, C.-T. A. Lee, Effects of crustal thickness on magmatic differentiation in subduction zone volcanism: A global study. *Earth Planet. Sci. Lett.* **470**, 96–107 (2017).
28. M. Chiaradia, Crustal thickness control on Sr/Y signatures of recent arc magmas: An Earth scale perspective. *Sci. Rep.* **5**, 8115 (2015).
29. J. Davidson, S. Turner, T. Plank, Dy/Dy*: Variations arising from mantle sources and petrogenetic processes. *J. Petrol.* **54**, 525–537 (2013).
30. H. Fujimaki, M. Tatsumoto, K.-I. Aoki, Partition coefficients of Hf, Zr and REE between phenocrysts and groundmasses, in *Proceedings of the Fourteenth Lunar and Planetary Science Conference* (Part 2 Journal of Geophysical Research, 1984), vol. 89, pp. B662–B672.
31. W.-Q. Ji, F.-Y. Wu, S.-L. Chung, C.-Z. Liu, The Gangdese magmatic constraints on a latest Cretaceous lithospheric delamination of the Lhasa terrane, southern Tibet. *Lithos* **210**, 168–180 (2014).
32. Z. Zajacz, P. A. Candela, P. M. Piccoli, C. Sanchez-Valle, The partitioning of sulfur and chlorine between andesite melts and magmatic volatiles and the exchange coefficients of major cations. *Geochim. Cosmochim. Acta* **89**, 81–101 (2012).
33. Z. Zajacz, The effect of melt composition on the partitioning of oxidized sulfur between silicate melts and magmatic volatiles. *Geochim. Cosmochim. Acta* **158**, 223–244 (2015).
34. M. Tang, M. Erdman, G. Eldridge, C.-T. A. Lee, The redox "filter" beneath magmatic orogens and the formation of continental crust. *Sci. Adv.* **4**, eaar4444 (2018).
35. K. A. Kelley, E. Cottrell, Water and the oxidation state of subduction zone magmas. *Science* **325**, 605–607 (2009).

36. H. Purwin, S. Lauterbach, G. P. Brey, A. B. Woodland, H.-J. Kleebe, An experimental study of the Fe oxidation states in garnet and clinopyroxene as a function of temperature in the system CaO–FeO–Fe_2O_3–MgO–Al_2O_3–SiO_2: Implications for garnet–clinopyroxene geothermometry. *Contr. Mineral. Petrol.* **165**, 623–639 (2013).
37. W. M. Nash, D. J. Smythe, B. J. Wood, Compositional and temperature effects on sulfur speciation and solubility in silicate melts. *Earth Planet. Sci. Lett.* **507**, 187–198 (2019).
38. M. Tang, C.-T. A. Lee, G. Costin, H. E. Höfer, Recycling reduced iron at the base of magmatic orogens. *Earth Planet. Sci. Lett.* **528**, 115827 (2019).
39. C. Chelle-Michou, B. Rottier, L. Caricchi, G. Simpson, Tempo of magma degassing and the genesis of porphyry copper deposits. *Sci. Rep.* **7**, 40566 (2017).
40. Y. Li, X.-H. Li, D. Selby, J.-W. Li, Pulsed magmatic fluid release for the formation of porphyry deposits: Tracing fluid evolution in absolute time from the Tibetan Qulong Cu-Mo deposit. *Geology* **46**, 7–10 (2018).
41. J. E. Mungall, Roasting the mantle: Slab melting and the genesis of major Au and Au-rich Cu deposits. *Geology* **30**, 915–918 (2002).
42. M. Chiaradia, Copper enrichment in arc magmas controlled by overriding plate thickness. *Nat. Geosci.* **7**, 43–46 (2014).
43. S. A. Crowe, G. Paris, S. Katsev, C. A. Jones, S.-T. Kim, A. L. Zerkle, S. Nomosatryo, D. A. Fowle, J. F. Adkins, A. L. Sessions, J. Farquhar, D. E. Canfield, Sulfate was a trace constituent of Archean seawater. *Science* **346**, 735–739 (2014).
44. A. D. Anbar, Y. Duan, T. W. Lyons, G. L. Arnold, B. Kendall, R. A. Creaser, A. J. Kaufman, G. W. Gordon, C. Scott, J. Garvin, R. Buick, A whiff of oxygen before the great oxidation event? *Science* **317**, 1903–1906 (2007).
45. R. M. Gaschnig, R. L. Rudnick, W. F. McDonough, A. J. Kaufman, Z. Hu, S. Gao, Onset of oxidative weathering of continents recorded in the geochemistry of ancient glacial diamictites. *Earth Planet. Sci. Lett.* **408**, 87–99 (2014).
46. K. O. Konhauser, S. V. Lalonde, N. J. Planavsky, E. Pecoits, T. W. Lyons, S. J. Mojzsis, O. J. Rouxel, M. E. Barley, C. Rosière, P. W. Fralick, L. R. Kump, A. Bekker, Aerobic bacterial pyrite oxidation and acid rock drainage during the Great Oxidation Event. *Nature* **478**, 369–373 (2011).
47. S.-J. Wang, R. L. Rudnick, R. M. Gaschnig, H. Wang, L. E. Wasylenki, Methanogenesis sustained by sulfide weathering during the Great Oxidation Event. *Nat. Geosci.* **12**, 296–300 (2019).
48. M. Tang, C.-T. A. Lee, R. L. Rudnick, K. C. Condie, Rapid mantle convection drove massive crustal thickening in the late Archean. *Geochim. Cosmochim. Acta* **278**, 6–15 (2019).
49. A. P. Beall, L. Moresi, C. M. Cooper, Formation of cratonic lithosphere during the initiation of plate tectonics. *Geology* **46**, 487–490 (2018).
50. H. Wang, J. van Hunen, D. G. Pearson, Making Archean cratonic roots by lateral compression: A two-stage thickening and stabilization model. *Tectonophysics* **746**, 562–571 (2018).
51. R. M. Garrels, A. Lerman, Coupling of the sedimentary sulfur and carbon cycles; an improved model. *Am. J. Sci.* **284**, 989–1007 (1984).
52. Y. Shen, R. Buick, D. E. Canfield, Isotopic evidence for microbial sulphate reduction in the early Archaean era. *Nature* **410**, 77–81 (2001).
53. J.-X. Li, K.-Z. Qin, G.-M. Li, B. Xiao, L. Chen, J.-X. Zhao, Post-collisional ore-bearing adakitic porphyries from Gangdese porphyry copper belt, southern Tibet: Melting of thickened juvenile arc lower crust. *Lithos* **126**, 265–277 (2011).
54. Y.-C. Zeng, J.-L. Chen, J.-F. Xu, M. Lei, Q.-W. Xiong, Origin of Miocene Cu-bearing porphyries in the Zhunuo region of the southern Lhasa subterrane: Constraints from geochronology and geochemistry. *Gondw. Res.* **41**, 51–64 (2017).
55. C.-B. Leng, X.-C. Zhang, H. Zhong, R.-Z. Hu, W.-D. Zhou, C. Li, Re–Os molybdenite ages and zircon Hf isotopes of the Gangjiang porphyry Cu–Mo deposit in the Tibetan Orogen. *Miner. Deposita* **48**, 585–602 (2013).
56. Y. Zheng, X. Sun, S. Gao, Z. Zhao, G. Zhang, S. Wu, Z. You, J. Li, Multiple mineralization events at the Jiru porphyry copper deposit, southern Tibet: Implications for Eocene and Miocene magma sources and resource potential. *J. Asian Earth Sci.* **79**, 842–857 (2014).
57. Z.-M. Yang, R. Goldfarb, Z.-S. Chang, Generation of postcollisional porphyry copper deposits in southern Tibet triggered by subduction of the Indian continental plate. *Econ. Geol. Spec. Publ.* **19**, 279–300 (2016).
58. S.-s. Sun, W. F. McDonough, Chemical and isotopic systematics of oceanic basalts: Implications for mantle composition and processes. *Geol. Soc. Lond. Spec. Publ.* **42**, 313–345 (1989).
59. M.-A. Fortin, J. Riddle, Y. Desjardins-Langlais, D. R. Baker, The effect of water on the sulfur concentration at sulfide saturation (SCSS) in natural melts. *Geochim. Cosmochim. Acta* **160**, 100–116 (2015).
60. P. King, R. Hervig, J. Holloway, J. Delaney, M. Dyar, Partitioning of Fe^{3+}/Fe_{total} between amphibole and basanitic melt as a function of oxygen fugacity. *Earth Planet. Sci. Lett.* **178**, 97–112 (2000).
61. V. Matjuschkin, J. D. Blundy, R. A. Brooker, The effect of pressure on sulphur speciation in mid- to deep-crustal arc magmas and implications for the formation of porphyry copper deposits. *Contr. Mineral. Petrol.* **171**, 66 (2016).
62. R. Wang, J. P. Richards, L.-M. Zhou, Z.-Q. Hou, R. A. Stern, R. A. Creaser, J.-J. Zhu, The role of Indian and Tibetan lithosphere in spatial distribution of Cenozoic magmatism and porphyry Cu–Mo deposits in the Gangdese belt, southern Tibet. *Earth Sci. Rev.* **150**, 68–94 (2015).
63. W.-Q. Ji, F.-Y. Wu, C.-Z. Liu, S.-L. Chung, Early Eocene crustal thickening in southern Tibet: New age and geochemical constraints from the Gangdese batholith. *J. Asian Earth Sci.* **53**, 82–95 (2012).

Acknowledgments: We thank G. Gaetani for handling the manuscript and three anonymous reviewers for constructive comments. We are grateful for discussions with Y. Shen, B. Wan, F. Wu, X. Chu, and W. Cao, Q. Mao's assistance in electron microprobe analysis and H. Zhang's assistance in collecting samples in Tibet. **Funding:** This work was supported by a U.S. NSF grant (EAR-1850832) to M.T. and C.-T.A.L. Field and analytical work was supported by a State Key Laboratory of Lithospheric Evolution grant (SKL-Z201706). **Author contributions:** M.T. designed the project and conducted the measurements with G.C. and W.-Q.J. M.T. and C.-T.A.L. wrote the manuscript. All authors contributed to data interpretation. **Competing interests:** The authors declare that they have no competing interests. **Data and materials availability:** All data needed to evaluate the conclusions in the paper are present in the paper and/or the Supplementary Materials. Additional data related to this paper may be requested from the authors.

Submitted 18 December 2019
Accepted 16 June 2020
Published 29 July 2020
10.1126/sciadv.aba6342

Citation: M. Tang, C.-T. A. Lee, W.-Q. Ji, R. Wang, G. Costin, Crustal thickening and endogenic oxidation of magmatic sulfur. *Sci. Adv.* **6**, eaba6342 (2020).

Science Advances

Crustal thickening and endogenic oxidation of magmatic sulfur

Ming Tang, Cin-Ty A. Lee, Wei-Qiang Ji, Rui Wang and Gelu Costin

Sci Adv **6** (31), eaba6342.
DOI: 10.1126/sciadv.aba6342